Biomass Conversion and Biorefinery
https://doi.org/10.1007/s13399-023-04645-4

ORIGINAL ARTICLE

Characterization of novel cellulosic fibers extracted from *Hibiscus canescens* stem

Raghuram Pradhan[1] · Basanta Kumar Palai[1] · Dhirendra Nath Thatoi[2] · A. Elayaperumal[3] · Japhia Sudarsan Nalla[1]

Received: 18 May 2023 / Revised: 5 July 2023 / Accepted: 15 July 2023

Abstract

Novel natural plant fibers are being extensively investigated at this current scenario mainly owing to their significant properties over synthetic ones as renewable, biodegradable, and economical nature. With this outlook, the present study has tried to explore a novel plant fiber from *Hibiscus canescens* stem and analyzed its feasibility through various characterization methods. Water retting method was elected to extract fibers from the *H. canescens* stem. Chemical analysis was used to determine various chemical components as cellulose, hemicellulose, lignin, wax, moisture, and ash. The crystalline and amorphous conformation of *H. canescens* stem fibers (HCSF) were discovered using X-ray diffraction analysis. The chemical possessions are further validated through Fourier transform infrared spectroscopy analysis. After physico-chemical investigation, the feasible properties of HCSF were determined to be good crystallinity (48.78%), high cellulose content (68.46 wt.%), and relatively low density (1425 kg/m^3). Moreover, the desired thermal stability (327°C) and tensile properties (394.9±14.42 MPa; 30.29±4.365 GPa) obtained through thermogravimetric analysis and tensile study demonstrated its suitability for high temperature fixed submissions. The exterior topographical study using SEM and AFM revealed that the surface is uneven with an average roughness of 7.200nm, which is another required feature for good fiber-matrix inter-bonding. Although, these intriguing features are satisfactory to ponder HCSF as a new promising material for composite fabrication in future.

Keywords *Hibiscus canescens* · Stem fiber · Reinforcement · Crystallographic analysis · Thermal analysis

1 Introduction

Synthetic fiber–based materials have been primarily employed for structural applications in most of the sectors, in the last few decades [1]. However, the current environmental policies looking over sustainable materials that cannot create any socio-ecological issues but ensure superior qualities, on the other hand. Since a revolution is necessary at this eco-concerned scenario to produce sustainable and biodegradable materials to replace traditional synthetic materials [2], natural plant fibers are one among the choice due to their cost-effective, biodegradable, renewable, and lightweight nature, which could be used for the fabrication of fiber reinforced polymer composites [3, 4]. Plant-based fibers provide several advantages while their ready availability is a major driving force in their increased adoption. Despite their low density, lower cost, eco-friendliness, and good thermal property, plant fibers have seen an uptick in use in recent years [5]. Sisal, jute, hemp, and cotton are just a few examples of plants that are grown primarily for their fiber, which has high economic importance. However, some fibers are obtained from agro-industrial residues as coir, maize stalk fiber, and sugar cane waste fibers [6]. The former ones are termed as primary fiber-yielding plants and later ones are termed as secondary fiber-yielding plants. Wood, silk, bamboo, hemp, sisal, flax, kenaf, and other common plant fibers were successfully reinforced with polymers, and the resulting composites exhibited better competitive properties [7].

However, the usage of low-quality plant fibers is limited in several domains due to the concerned issues including poor temperature resistance, excessive water

✉ Basanta Kumar Palai
basantapalai01@gmail.com

[1] Department of Mechanical Engineering, GIET University, Gunupur, Rayagada, Odisha 765022, India

[2] ITER, SOA deemed to be University, Bhubaneswar, Odisha 751030, India

[3] Engineering Design Division, College of Engineering, Guindy, Anna University, Chennai, Tamilnadu 600025, India

Published online: 24 July 2023

captivation, incompatibility, and aggregation tendency. Since identifying novel high-quality fibers is still a challenging task because of the variations in the fiber components particularly, cellulose, hemicellulose, lignin, and moisture content among different fiber sources [8]. The majority of the time, fibers are utilized not in their raw or unprocessed states but rather in the form of blends. Blends of fiber and polymers exhibited good qualities when compared to synthetic fibers. Ropes, insulations, textiles, and polymer composites are just few of the many products that find usage for plant fibers in their raw/blended forms. Flax and jute fibers are often used in direct rope-making methods [9]. Yarns, on the other hand, found in things like clothes, purses, and even carpets, and they are often woven from a variety of plant fibers. Needle felts made from coir fibers are great for absorbing sound and blocking out unwanted noise when used as acoustic soundproofing [10]. Biodegradable flower pots, briefcases, bookshelves, table tops, disc holders, seats, and even wind generators, vehicles, airplanes, etc. all make use of natural fibers, which are widely acknowledged as reinforcing materials in the composites sector [11].

Fiber-reinforced composites are often produced by reinforcing two or more materials together, which ultimately leads in the production of a composite with desirable qualities extracted from the usual materials that were blended [12]. In most cases, it will be made up of a material that has a continuous phase, into which one or more discontinuous phase (reinforcing phase) components will have been placed. The discontinuous phase of composites is created by the reinforcing material or fibers, which are typically reinforced into the matrix in a scattered manner. Because the matrix ensures that the reinforcement remains precisely where it should be in order to provide the composite with sufficient mechanical properties [13]. Furthermore, the surface roughness of the fiber has a significant impact on the interfacial bonding between the fiber and matrix. Even though, a composite's ultimate strength is dependent on the reinforcements' qualities, distribution, interactions, as well as the proportion by weight or volume that used to fabricate the composite, where the geometry of the reinforcing phase as shape, size, and distribution are profoundly have influence on composite properties. Thermoset and thermoplastic polymer matrices may be used as continuous phase for composite fabrication through any of the injection molding, compression molding, melt-extrusion, and hand lay-up techniques [14].

However, identification of a high-quality fiber or reinforcement is still recognized as a challenge in fiber-based material research. The identification of a suitable fiber source, optimization of extraction procedure, fiber modification through pretreatments, and its characterization are the main milestones of fiber research. Generally, water retting and dew retting are used widely for the extraction methods for plant fibers. In this study, water retting method was employed for the extraction of fibers. Fiber pretreatment is effective in case of many fibers to improve their specific properties by delignification. Pretreatments separate non-cellulosic components as lignin, wax, and hemicelluloses from the lignocellulose network. However, the cost of pretreatment techniques relies as the constraint of this aspect. Many researchers are evaluating plant fiber-reinforced polymer composites to evaluate their performance and appropriateness in a variety of applications [15]. This high demand for cellulosic fibers has prompted the authors to look over *Hibiscus canescens* stem for fiber extraction and its characterization to establish the feasibility of relevant fibers for composite applications. There is no study reported on the characterization of *H. canescens* stem fiber still now. Although, this article compares *H. canescens* stem fiber to other plant fibers in terms of its density, diameter, tensile qualities, chemical composition, crystallographic properties, thermal properties, and surface morphological features to establish the efficacy of proposed fiber for composite applications.

2 Materials and methods

2.1 Plant collection and fiber extraction

Hibiscus canescens is a dicotyledonous shrub commonly named as grayish Hibiscus, which is native to warm, temperate, subtropical, and tropical regions. They belong to the family Malvaceae and are widely distributed in Africa and South Asia, especially in certain regions of India. The mature *H. canescens* plants were gathered from a Village in the Madurai district of Tamil Nadu of South India. Water retting method was employed in this study to extract fibers from *H. canescens* stem. For that, the collected plant stems were made devoid of all other plant parts and washed thoroughly to remove external particles, if any. After being washed, the plant stems were submerged in the water filled in a container for 2 weeks. This could result microbial degradation and consequently fibers enclosed with retted material were detached through manual combing using a metal brush. Subsequently, the fibers obtained through retting procedure were taken out of the container and rinsed carefully with purified water to get rid of any remaining contaminants. The fibers were then sun dried for 7 days and further dried in an oven for 24 h to eliminate the residual moisture content [16]. Figure 1 depicts the plant that is utilized for fiber extraction (a), retted material obtained after water retting (b, c) and fibers attained after manual combing (d).

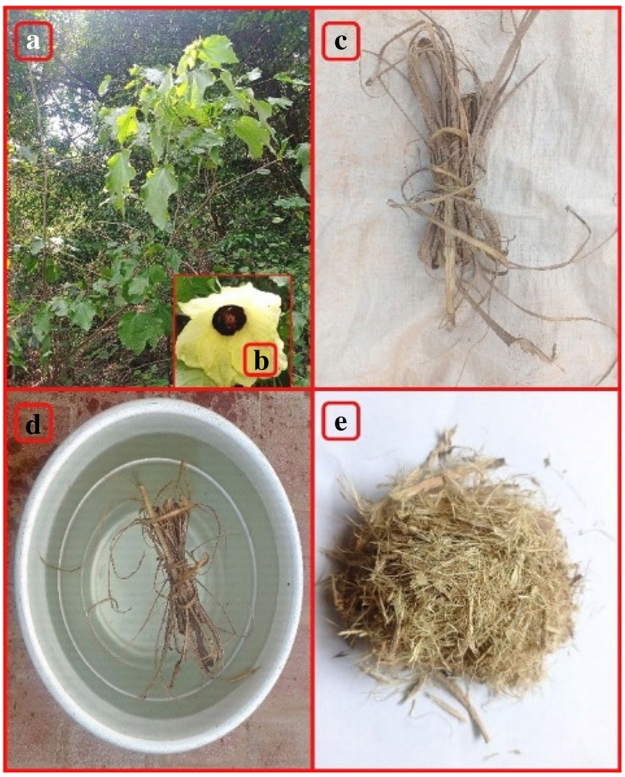

Fig. 1 *Hibiscus canescens* plant (**a**), retted material (**b**, **c**), and extracted fibers (**d**)

2.2 Characterization of *Hibiscus canescens* stem fiber (HCSF)

For determining the fiber's appropriateness for lightweight purposes physical examination is necessary in terms of density and diameter analysis. Insights on understanding the fiber's composition, functional groups, and crystallinity, chemical analysis is admirable. The mechanical and thermal properties of the fiber can be determined with sufficient accuracy using the tensile and thermal tests. To measure surface roughness characteristics of the fiber to assess its interbonding capability, morphological investigation is preferred. Since the extracted raw fibers (HCSF) were subjected for a group of tests mentioned above to determine its suitability for use in diverse composite formulation.

2.3 Physical properties analysis

The diameter of and the density of were the two different aspects of its physical make-up that were looked at during this study utilizing the procedures that were outlined below. The cross-sectional area of the HCSF fiber was measured at four different places along its length by subjecting it an Auslese 7 LCD digital optical microscope. A total of 20 fiber samples were tested, and the average diameter of the specimens was determined using the image-pro program due to its irregular cross-sectional area. For density measurement, a pycnometer was used, where methylbenzene was cast-off as a known density liquid instead of toluene. The following equation was used to calculate density (1) of HCSF; specifically, m_1 represents the mass (kg) of the unoccupied pycnometer, m_2 represents the weight (kg) of the pycnometer after being subjected to fiber, m_3 represents the mass (kg) of the pycnometer after being filled with methylbenzene, m_4 represents the density (kg) of pycnometer which is filed with HCSF and methylbenzene, and ρ_{MAPF} (g/cm^3) corresponds to the density of HCSF [17].

$$\rho_{(\mathrm{MAPF})} = \left(\frac{m_2 - m_1}{(m_3 - m_1) - (m_4 - m_2)} \right) \rho_m \tag{1}$$

2.4 Thermal performance of HCSF

The thermal study was performed to establish the appropriateness of fiber for high temperature necessitate dealing and applications, specifically to identify the thermal stability and maximum degradation temperature of the proposed material. This investigation was carried out using a NETZSCH STA 449F3 thermal analyzer, in which a 5.458mg of HCSF sample was placed in an alumina plate and heated from 32 to 600°C at a rate of 10°C/min [18]. Nitrogen gas (N2) was infused into the system at a rate of 30 ml/min to uphold an inert atmosphere that assist to overcome oxidation effects during inspection[19, 20]. The resultant TG/DTG curves were recorded which displays the thermal degradation profile of HCSF in terms of weight loss of HCSF against increasing temperature ranges. Furthermore, the kinetic activation energy of the material (E_a) was estimated through Briodo's curve in accordance with Broido's equation (2). In Broido's equation, the universal gas constant is represented as R that is equal to 8.314 J/mol K, temperature in Kelvin is signified by T, reaction constant is embodied by K and the normalized weight (weight at any time (W_t)/initial weight (W_i)) is indicated by y [21].

$$\ln\left[\ln\left(\frac{1}{y}\right)\right] = -\left(\frac{E_a}{R}\right)\left[\left(\frac{1}{T}\right) + K\right] \tag{2}$$

2.5 Tensile characterization

Mechanical behavior of HCSF was investigated with the aid of Zwick/Roell universal testing equipment. For that, fiber samples were prepared as per ASTM D3822-07 specifications 1kN load cell, Instron 5500 R testing machine was used at room temperature condition with a total of 20 single fiber samples with a gauge length of 50 mm were investigated for

understanding the variations in tensile properties, due to the uneven nature of fiber. All the samples were run at a cross-head speed of 2.5mm/min during the examination [15]. The reliability of tensile characteristics of 20 fiber samples were evaluated through Weibull distribution curves using the software Minitab-17 [22]. The microfibril angles (α) of HCSF was further determined using the following relation (3) [23]. Of which, strain is represented by the symbol ε, microfibril angle (°) is given as α, while the change in length-at-break is shown by ΔL (mm).

$$\varepsilon = \ln\left(1 + \frac{\Delta L}{50}\right) = -\ln(\cos\ \alpha) \tag{3}$$

2.6 Chemical examination

2.6.1 Chemical composition of raw MAPF

Through the use of conventional chemical analysis procedures, the composition of various chemical components of HCSF were detected. According to Kurshner and Hoffer's method, the amount of cellulose in the HCSF was determined [24]. Hemicellulose content was evaluated using the neutral detergent fiber method, as per [25]. Estimation of the sample's lignin concentration followed the standard approach established by APPITA P11s-78 [26, 27]. The wax concentration in the HCSF was investigated using the Conrad method, for that, the waxy residue obtained after treating crushed fiber samples with ethanol and then chloroform was weighed [28]. Similarly, ash fraction of the material was determined using the TAPPI (Technical Association of the Pulp and Paper Industry) standard [29]. A Mettler Toledo HS153 moisture analyzer was employed to check the moisture percentage of HCSF, and the average moisture content was noticed while analyzing 10 trials for each fiber samples[30, 31].

2.6.2 FT-IR characterization

FT-IR analysis was used to study the major functional groups associated with each individual chemical component of HCSF in order to determine the chemical conformation of the compound. This procedure was done with the aid of a Jasco FT-IR 6300 type-A spectrometer, to which a thin film of HCSF powder and potassium bromide (1:10) being subjected. During examination, 32 scans were taken per minute at a resolution of 4 cm^{-1}, within a wave number range of 4000 to 500 cm^{-1} [32]. All scans were performed at a constant 2 mm/s scanning speed and 45° incidence angle [1]. The conduction percentage of diverse functional groups occupied in the material was recorded as FT-IR spectra, which was used to authenticate the constituent parts of the fiber [33].

2.6.3 Crystallinity analysis

X-ray diffraction (XRD) analysis was conducted to authenticate the existence crystalline and amorphous fractions in the fiber sample. This examination was executed in an X' Pert PRO diffractometer, where powdered HCSF sample was subjected to a sample holder, followed by X-rays (CuK) with an intensity of 1.5406A passed through the material, and the corresponding diffracted rays were recorded using an X-ray detector in the 2θ range (10°–50°) with a scan rate and speed rate of 10.0231° to 80.9231°, 1°/m, respectively. According to peak height method, the crystallinity index (CI) of the HCSF was derived through Siegal's formula (4). Of which, I_{am} is given to represent the intensity of amorphous peak at 18°, I_{002} signify the possession of the crystalline peak at 23° [34]. Additionally, the crystallite size of HCSF was determined using Sherrer's formula (5), where β denotes the whole width at half maximum of the peak at 23°, λ represent the radiation intensity, K denotes the universal constant (0.89), and θ is the Bragg angle [35].

$$\mathrm{CI} = \left(1 - \frac{I_{am}}{I_{002}}\right) \times 100\% \tag{4}$$

$$\mathrm{CS} = \frac{K\lambda}{\beta \mathrm{Cos}\theta} \tag{5}$$

2.7 Surface topographies of MAPF

The imaging techniques as SEM (scanning electron microscopy), EDX (energy-dispersive X-ray spectroscopy), and AFM (atomic force microscopy) were used to evaluate the fiber's roughness characteristics and elemental dispersal [5]. The methods used to inspect surface properties of HCSF are explicated in the following sections.

2.7.1 SEM investigation

The surface features of the HCSF sample were accomplished in the longitudinal direction by using a SEM model FEI Quanta FEG 200. In order to increase the conductivity of the fiber and thus to lower the over shielding effect of electrons, the specimens were coated with a thin film of gold prior to examination. Then, high-resolution images of HCSF surface were captured at four different magnifications as 200×, 500×, 1000×, and 2000×. The experiment was conducted in the low-vacuum mode (50 Pa) at an accelerating voltage of 15kV. It was probable to identify the microstructures present on the exterior part of the fiber using obtained images. Also, the images were sufficient to establish the surface roughness/smoothness and its inter-bonding capacity to a certain extent [36].

2.7.2 EDX spectroscopic analysis

The energy-dispersive X-ray spectroscopy (EDX) was used to reveal the most notable elements present on the exterior part of the fiber. The elemental quantification was performed using an EDX spectrometer type NCAPentaFET83 coupled with a high-resolution SEM equipment. The resultant spectrum was obtained through an EDX detector, which shows the prominence of individual elements existing on the fiber surface, in term of atomic and weight percentage [37].

2.7.3 Atomic force microscopic (AFM) examination

Using an AFM (Park, Korea, model XE-70), quantification of diverse surface roughness parameters was done. The examination has realized with non-contact mode, where a shielding frequency of 293 Hz and an accuracy of 1nm was used. The acquired 3D/2D images were further processed with XEI image processing software that is connected to the AFM. The parameters as average surface roughness (R_a), root mean square roughness (R_q or R_{rms}), 10-point average roughness (R_z), surface skewness (R_{sk}), surface kurtosis (R_{ku}), and maximum peak-to-valley height (R_t) were quantified through this way and which was adequate to describe the peripheral roughness of HCSF [38].

3 Results and discussion

The physico-chemical, mechanical, thermal, and morphological characteristics of HCSF are described in detail in this session. The significant research outcomes are presented in the form of figures and tables, where appropriate comparisons are made with existing fibers to explore the position of proposed fiber.

3.1 Physical properties of HCSF

The diameter variations of four randomly selected regions of a HCSF are depicted in Fig. 2, which is an optical microscopic view. Due to the irregular weaving of the fibers, an average diameter of 441.32 µm was calculated after analyzing 20 separate HCSF samples. Generally, fibers with moderate diameter are favored due to the fact that moderate diameter offer good tensile properties, whereas high diameter leads to fiber-matrix incompatibility and low diameter causes reduced tensile strength. The diameter found to be moderate when compared to other investigated fibers such as *Tamarindus indica* (564–789 µm), *Prosopis juliflora* (20 µm), *Phaseolus vulgaris* (535.6 µm), Sisal (50–300 µm), *Coccinia grandis* (27.33 µm), date palm rachis (520 ± 72 µm), *Ficus religiosa* root (0.09–0.12 µm), kenaf (65–71 µm), *Pongamia pinnata* (62.34 µm), Ramie (50 µm), Juncus (3300 µm), *Cissus quadrangularis* stem (770–870 µm), purple *Bauhinia purpurea* (511± 3.07 µm), and *Cissus quadrangularis* root (610–725 µm). The density (1425 kg/m^3) of HCSF beheld promising when compared to other fibers including purple *Bauhinia purpurea* (1460 kg/m^3), *Coccinia grandis* (1517 kg/m^3), *Cissus quadrangularis* root (1510 kg/m^3), flax (1500 kg/m^3), pine apple leaf fiber (1440 kg/m^3), hemp (1500 kg/m^3), sisal (1500 kg/m^3), cotton (1600kg/m^3), and glass fibers (2500 kg/m^3) [17, 39]. A low density and a reasonable diameter of fibers are essential requirements

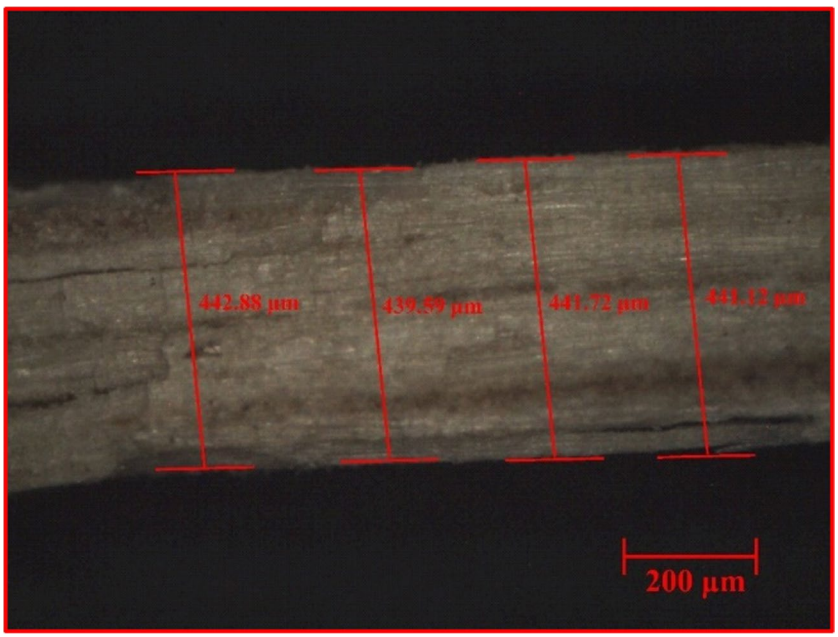

Fig. 2 Diameter variations of HCSF

in the making of lightweight products. These two studies, however, demonstrate the physical suitability of fiber for use in lightweight composites. Table 1 presents the physical properties of HCSF and other comparable fibers, along with their other specific properties.

3.2 Thermogravimetric analysis of HCSF

The weight loss feature of HCSF owed by thermal degradation is depicted in Fig. 3 (a, b, c), which illustrates the TG/DTG curves (a) and differential thermal analytic (DTA) curve (b). It is clear from the outcomes that the initial stage of mass loss was occurred around 70°C, and is indicative of the evaporation of existing water content from the HCSF. Between the temperature range of 200–321°C, the degradation of hemicellulose component is validated and which indicates the second stage of degradation. In 2020, Palai and Sarangi observed a similar deterioration pattern in plant fiber. The third phase of weight loss occurred in between 375 and 500°C that represent the elimination of cellulose fractions. Hence the thermal stability of HCSF is identified as 375°C. Even after being heated to 500°C, maximum degradation of sample has been occurred around 550°C. Similar pattern of degradation was observed through DTA analysis that also validated TGA results in terms of proving the complete hemicellulose and cellulose degradation drift at 321°C and 454–486°C. In addition, this experiment established that HCSF is stable up to 250°C, an essential attribute that makes the fiber suitable for high heat environments. However, the thermal stability of HCSF is promising than the thermal resistance of *Tamarindus indica* (238°C), *Ricinus communis* (225°C), *Passiflora foetida* (320°C), *Pongamia pinnata* (332°C), *Phaseolus vulgaris* (328.5°C), *Phoenix dactylefera* L. leaf sheath (245.1°C), *Cissus quadrangularis* root (230°C), *Cissus quadrangularis* stem (270°C), *Prosopis juliflora* (217°C), *Coccinia grandis* (213.4°C), *Cymbopogon flexuous* (253.17°C), *Zmioculus zamiifolia* (310 ± 2.64°C), *Ficus religiosa* (325°C), *Phaseolus vulgaris* (328.5°C), sisal (250°C), hemp (225°C), *Juncus effuses* L. (200°C), cotton (265°C), *Altheria officinalis* L. (320°C), *Tridax procumbens* (195°C), and *Thespesia populnea* (245.4°C) (Table 2). Moreover, the revealed thermal stability of HCSF is imperative since that allow the fiber to be appropriate for high thermal settings. Kinetic activation energy (E_a), on the other hand, is the minimal amount of energy needed to commence the disintegration of cellulosic fibers and is used to evaluate the degradation pattern of plant fibers. A typical range of kinetic activation energy of plant fiber is 60–170 kJ/mol. The kinetic activation energy of HCSF (65.66 kJ/mol) calculated using Broido's plot (c) is in the required range, which was almost closer to the activation energy reported for *Grewia damine* (65.29 kJ/mol) (Indran et al., 2014; Umashankaran and Gopalakrishnan, 2019).

3.3 Tensile features of HCSF

Usually, different fibers beheld different tensile properties that dramatically affects the mechanical strength of its reinforced polymers. Hence, tensile characterization of HCSF was done, where the fibers with 40mm length showed maximum tensile features as displayed in Table 3. The tensile strength of the 40mm HCSF is identified as 394.9 ± 14.42 MPa, which is higher than the mechanical strength of *Ricinus communis* (356 ± 2.387 MPa), *Juncus* (31 ± 8 MPa), *Coccinia grandis* (273 ± 2.74 MPa), *Juncus effuses* L. (113 ± 36 MPa), *Tridax procumbens* (25.75 MPa), *Acacia concinna* (302.1 ± 16.78 MPa), *Zmioculus zamiifolia* (34.92 ± 5.47 MPa), *Pongamia pinnata* (322 MPa), purple *Bauhinia purpurea* (373.3 MPa), and *Grewia damine* (375.6 ± 16.58 MPa). Significant tensile modulus was recognized for HCSF (30.29 ± 4.365 GPa) because of its superiority over the average tensile modulus of *Tamarindus indica* (11.23 ± 2.72 GPa), *Juncus* (0.7 ± 0.1 GPa), *Pongamia pinnata* (9.67 GPa), *Coccinia grandis* (10.17 ± 1.26 GPa), *Zmioculus zamiifolia* (0.135 ± 0.052 GPa), kenaf (25.1 GPa), *Acacia concinna* (8.544 ± 0.210 GPa), *Juncus effuses* L. (4.38 ± 1.37 GPa), purple *Bauhinia purpurea* (5.31 GPa), and *Tridax procumbens* (0.94 ± 0.09 GPa). The strain at break of HCSF was found to be 5.32 ± 0.34% and a microfibril angle of 18.53 ± 0.582° was noted. Recent studies on manau rattan (*Calamus manan*) fibers revealed the utility of fibers for optical fiber production due to its good thermal resistance (332°C), tensile (273–482.6MPa), and transparent features. Similar thermal (321°C) and tensile features (394.9 ± 14.42MPa) noted for HCSF too. Moreover, all the potential mechanical and thermal features observed have disclosed that HCSF could be a better candidate for such kind of composite preparation.

The Weibull distribution plots corresponding to diameter (a), tensile strength (b), tensile modulus (c), and stress–strain rate (d) are presented in Fig. 4, which clearly show how dramatically plant fibers tensile properties can alter. All the four tensile value deviations were found to be within the Weibull range, proving that HCSF may be successfully used as reinforcement in polymer composites. The amount of surface porous and chemical constituents' integrity, the critical length of this HCSF at 40mm were observed. This 40-mm fiber length can be used as a discontinuous reinforcement with polymeric composite materials.

3.4 Chemical components of HCSF

High cellulose content of 68.46 wt.% observed for HCSF suggesting it holds excellent crystallinity along with good thermal and tensile properties, as already established through thermal and tensile tests. Compared to other

Table 1 Physico-chemical composition of HCSF in comparison with other natural fibers

Fiber name	Physical properties		Chemical properties						Crystalline properties		References
	Diameter (μm)	Density (kg/m^3)	Cellulose (Wt.%)	Hemi celluloses (wt.%)	Lignin (wt.%)	Wax (wt.%)	Moisture Content (wt. %)	Ash (wt.%)	CI (%)	CS (nm)	
Hibiscus canescens stem fiber	441.32	1425	68.46	14.36	12.48	0.28	10.44	5.34	48.78	1.59	Present study
Prosopis juliflora bark	20	580	61.65	16.14	17.11	0.61	9.48	5.2	46	2.8	[40]
Cymbopogon flexuosus root	460	1330	58.33	9.76	27.50	0.42	8.70	4.91	36.8	13.96	[41]
Coccinia grandis	27.33	1243	62.35	13.42	15.61	0.79	5.6	4.388	52.17	13.38	[42]
Arundo donax	-	1168	43.2	20.5	17.2 -	-	-	1.9	-	-	[43]
Althaea officinalis L.	156–194	1180	44.6	13.5	2.7	-	-	2.3	68	2.4	[44]
Acacia planifrons	-	660	73.1	9.41	12.04	0.57	8.21	4.06	65.38	-	[45]
Acacia arabica	-	1028	68.10	9.36	16.86	0.49	-	-	51.72	15	[45]
Sida rhombifolia	-	1320.7	75.09	15.43	7.48	0.49	12.02	4.07	56.6	2.75	[46]
Root of *Ficus religiosa* tree	25.62	1246	55.58	13.86	10.13	0.72	9.33	4.86	42.92	5.18	[47]
Ramie	50	1500	76	15	1	-	8.0	-	58	16	[47]
Lygeum spartum L.	180–433	1499.7±3.1	-	-	-	-	-		46.19	-	[48]
Kenaf	65–71	1400	53.14	14.33	8.18	0.8	6.2–12	2–5			[47]
Juncus effuses L.	1.139	280	-	-	-	-	-	-	33.4	3.6	[49]
Flax	-	1500	85	09	4	1.7	10	-	70	5.4	[50]
Ferula communis	-	-	53.3	8.5	1.4	-	-	-	48	1.6	[51]
Artisdita hystrix	-	540	59.54	11.35	8.42	-	-	-	44.85	-	[52]
Cotton	-	1600	85–90	1–3	0.7–1.6	-	1.0		68	5–7	[53]
Heteropogon contortus	-	602	64.87	19.34	13.56	0.22	7.4	-	54.1	-	[6]
Bamboo	240–330	910	26–43	30	1–31	-	9.16	-	-	-	[47]
Coccinia grandis stem	543–621	1517.5	63.22	-	24.42	0.32	9.14	-	46.09	1.91	[54]
Areca palm leaf stalk	285–330	1090 ± 24	57.49 ± 0.66	18.34 ± 0.24	7.26 ± 0.12	0.71 ± 0.024	9.35 ± 0.15	1.43 ± 0.019	-	-	[55]
Mulberry barks	-	-	37.38 ± 2.31	25.32 ± 2.45	9.99 ± 0.82	-	-	-	58.8	-	[56]
Thespesia populnea	87–256	1412	70.2	12.64	16.34	0.76	10.83	1.80	48.17	3.576	[57]
Tridax procumbens	233.1±9.9	1.16±0.12	32	6.8	3	0.71	11.2		34.46	25.04	[50]
Triticum (wheat straw)	-	-	51	26	15	-	-	-	54.42	-	[58]

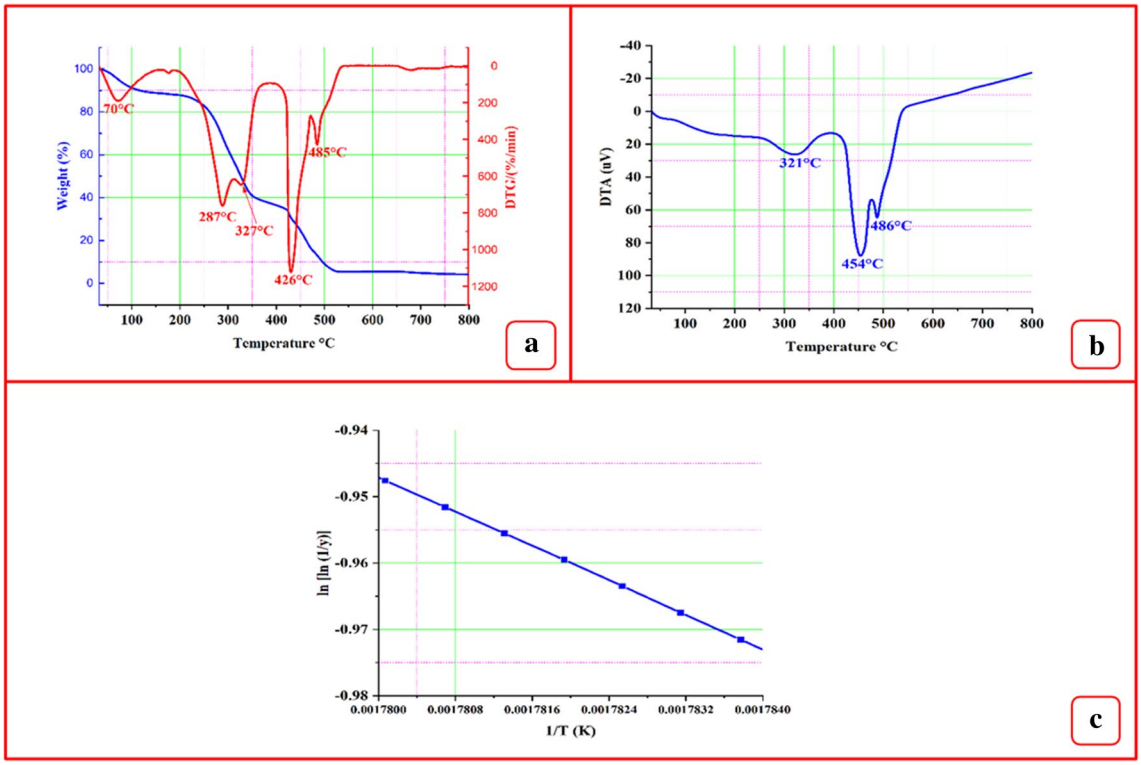

Fig. 3 TGA/DTG curves (**a**), DTA curve (**b**), and Broido's plot (**b**) of HCSF

cellulosic fibers such as *Grewia damine* (57.78 ± 3.56 wt.%), *Ficus religiosa* (55.58 wt.%), *Acacia concinna* (59.43 wt.%), purple *Bauhinia purpurea* (60.54 ± 4.31 wt.%), *Zmioculus zamiifolia* (41.12 ± 3.32 wt.%), *Coccinia grandis* L. (63.22 wt.%), *Phoenix dactylefera* L. leaf sheath (43.50 wt.%), *Prosopis juliflora* (61.65 wt.%), *Tridax procumbens* (32 wt.%), *Cymbopogon flexuous* (68.13 wt.%), *Ricinus communis* (65.5 wt.%), *Pongamia pinnata* (62.34wt.%), *Altheria officinalis* L. (44.6 wt.%), *Phaseolus vulgaris* (62.17 wt.%), and jute, HCSF (58–63 wt.%) was promising due to its high cellulose content [6]. The proportion of other components in HCSF were 14.36 wt.% (hemicelluloses), 12.48 wt.% (lignin), 0.28 wt.% (wax), 10.44 wt.% (moisture), and 5.34 (ash). In fact, the low hemicellulose and lignin concentration found in fiber point towards its high tensile and lower moisture absorption properties; which also indicate that the fiber possess less amorphous fraction and is resistant to water or moisture [9, 17]. At the same time, low moisture (10.44 wt.%) content was detected for HCSF that disclosed the long-term durability of fiber, which is advantageous than typical fibers as jute (10.99 wt.%), hemp (10.8 wt.%), sisal (11 wt.%), *Tridax procumbens* (11.2 wt.%), *Thespesia populnea* (10.83 wt.%), and pineapple leaf fiber (11.8 wt.%) [59, 60]. In general, the bonding effectiveness between plant fibers and polymer resin could be lower when a higher wax content is present in the fibers. Since low wax concentration (0.28 wt.%) noted for HCSF is an additional feature that portends well for its bonding with matrix, a relatively low ash concentration of 5.34 wt.% is found in fiber, which also reveals that the fiber possesses low amorphous content. The chemical make-up of HCSF is displayed in Table 1 along with those of similar fibers for easy comparison. In order to verify the accuracy of these qualitative results, further chemical validations were done using FT-IR, XRD, and NMR analysis.

3.5 Crystalline possessions of HCSF

X-ray diffraction spectra of HCSF sample reveals three significant peaks at 18.14°, 22.11°, and 34.59°, as seen in Fig. 5. The peak at 18.14° related to the lattice plane (1 1 0), and another peak between 22.11° relates to the cellulose I plane (2 0 0). An alignment of the fiber bundles was seen to produce minor peaks at 34.59° [4, 41]. Desired cryatallinity index (CI) and crystallite size was measured for HCSF as 48.78%, 1.59nm, respectively. At higher crystallinity, the cellulose chains become more consistently oriented, enhancing the mechanical qualities and makes them appropriate for biocomposites.

Table 2 Mechanical and thermal composition of HCSF in comparison with other natural fibers

Fiber name	Mechanical properties				Thermal properties		References
	Tensile strength (MPa)	Young's modulus (GPa)	Elongation at break (%)	Microfibril angle (°)	Thermal stability (°C)	Max degradation temperature (°C)	
Hibiscus canescens stem fiber	394.9±14.42	30.29±4.365	5.32±0.34	4.72±0.21	250	454	Present study
Prosopis juliflora bark	-	-	-	-	-	331.1	[40]
Cymbopogon flexuosus root	315.22± 61.72	4.77± 0.34	6.6± 2.7	4.3±0.21	272.31	309	[41]
Coccinia grandis	273±27.74	10.17±1.261	2.703±0.2736	13.25±0.664	213.4	351.6	[42]
Arundo donax	248	9.4	3.24	6.85± 1.23	275	320	[43]
Althaea officinalis L.	415.2	65.4	3.9	-	220	344	[44]
Acacia planifrons	-	-	-	-	200	362.4	[45]
Acacia arabica	-	-	-	-	-	345.1	[45]
Sida rhombifolia	673 ± 14	-	-	-	250	433.3	[46]
Root of *Ficus religiosa* tree	433.32 ± 44	5.42 ± 2.6	8.74 ± 1.8	-	325	400	[47]
Ramie	8.0870	128	1.2	-	-	-	[47]
Lygeum spartum L.	64.63–280	4.47–13.27	1.49–3.74	12.65 ±2.85	220)	338.7	[48]
Kenaf	470–785	25.1	1.75–1.9	-			[47]
Juncus effuses L.	113 ± 36	4.38 ± 1.37	2.75 ± 0.68	-	200	300	[49]
Flax	400-938	61.4-128	3.6 -3.8	-	-	-	[50]
Ferula communis	475.6 ± 15.7	52.7 ± 3.7	4.2 ± 0.2	-	200	313.5	[51]
Artisdita hystrix	440±13.4	1.57± 0.04	-	12.64±0.45	-	298.8	[52]
Cotton	287-597	5.5–12.6	7–8	-	265	280	[53]
Heteropogon contortus	476 ± 11.6	48 ± 2.8	1.63 ± 0.06	-	220	337.7	[6]
Bamboo	503	35.91	1.4	-	-	-	[47]
Coccinia grandis stem	424.242	26.515	16	-	105	320	[54]
Areca palm leaf stalk	364.66 ±21.46	9.39 ±1.13	3.47 ±1.15	-	110	365	[55]
Mulberry barks	-	-	-	-	210	250	[56]
Thespesia populnea	557.82 ±56.29	20.57 ±4.46	2.80 ±0.56	13.94 ±1.21	245.4	323.76	[57]
Tridax procumbens	25.75	0.94±0.09	2.77±0.27	13.4±0.64	195	250-350	[50]
Triticum (wheat straw)	-	-	-	-	-	-	[58]

Table 3 Tensile properties of HCSF with different length proportion

Fiber length	Tensile strength (MPa)	Young's modulus (GPa)	Strain to failure (%)
10mm	322.55±12.66	20.56±3.16	3.12±0.78
20mm	345.72±10.17	22.84±3.68	4.31±0.64
30mm	365.44±13.12	26.12±4.56	4.88±0.88
40mm	394.9±14.42	30.29±4.365	5.32±0.34
50mm	386.66±9.61	27.42±2.61	4.26±0.86

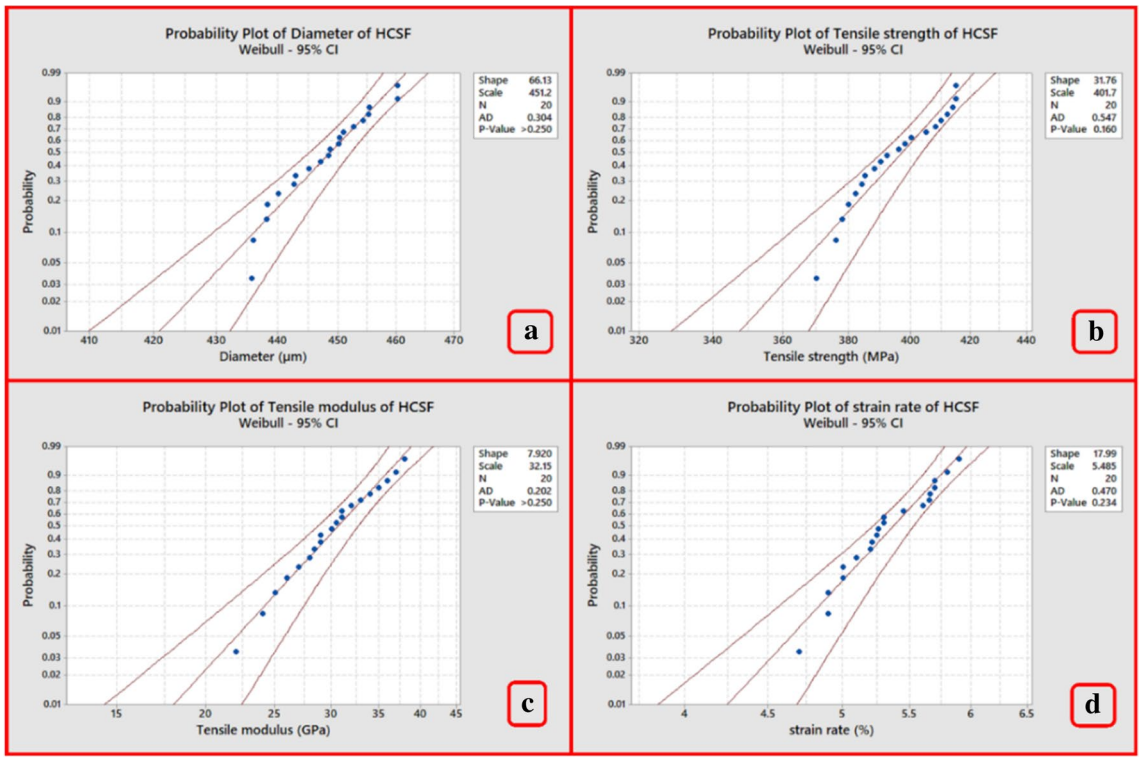

Fig. 4 Weibull plots of diameter (**a**), tensile strength (**b**), tensile modulus (**c**), and stress–strain rate (**d**) for HCSF

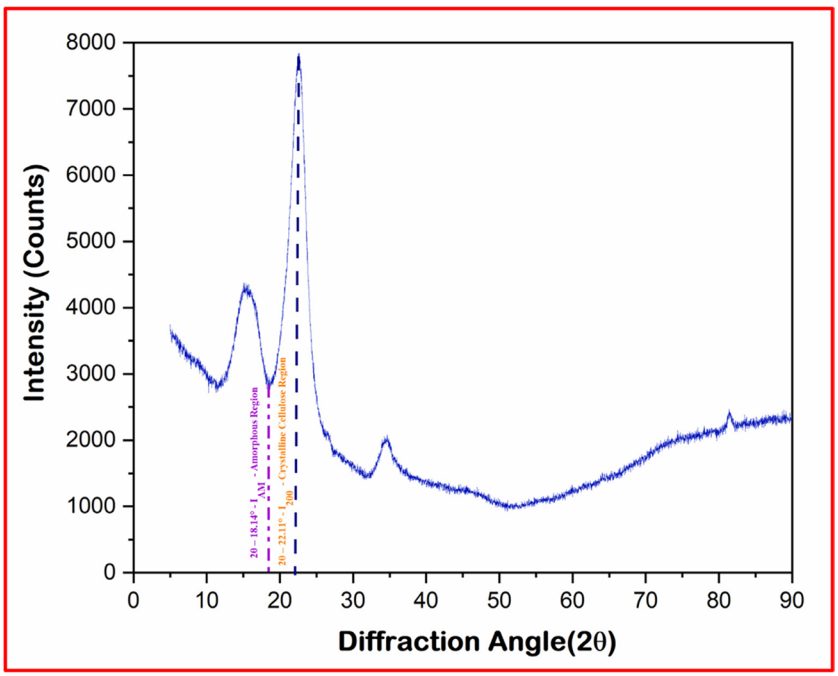

Fig. 5 X-ray diffractogram of HCSF

Larger crystalline size affects cellulosic fiber absorption and chemical reactivity. Thus, the observed cryatalline properties of this fibers were significant when compared to the other investigated natural fibers such as *Grewia damine* (30.35%, 5.09nm), *Ficus religiosa* (42.92%, 5.18nm), *Acacia concinna* (27.5%, 4.17nm), *Zmioculus zamiifolia* (25.75 ± 2.34%, 2.54 ± 0.24nm), *Prosopis juliflora* (46%, 2.8nm), *Tridax procumbens* (34.46%,

25.04nm), *Cymbopogon flexuous* (46.02%, 13.96nm), *Pongamia pinnata* (45.31%, 5.43nm), *Juncus* (43%), *Cissus quadrangularis* stem (47.1%), *Juncus effuses L.* (33.4%, 3.6nm), and *Thespesia populnea* (48.17%, 3.57nm) [9, 61, 62]. Moreover, the obtained diffractogram was appropriate to prove the occurrence of crystalline and amorphous components in the sample, which was also predicted through chemical composition analysis.

3.6 Functional groups of HCSF

Figure 6 displays the FT-IR spectrum of HCSF, demonstrating ten prominent peaks in different wavenumber zones, each of which is connected with a distinct functional group in the compound's chemical make-up. The first two peaks noted at 3335cm^{-1} and 2916 cm^{-1} is coupled with the cellulose component of fiber, which was attributed by the OH and CH stretching of cellulose [13]. The presence of α-cellulose in the fiber was sensed by noticing the peak at 2832 cm^{-1} that corresponds to the associated C-H stretching of alkanes. The following peak located at 2317cm^{-1} indicates C≡C groups due to the existence of wax in the sample. Likewise, the C=O (1611cm^{-1}) and C-OH (1021cm^{-1}) stretching noted in the FT-IR spectra is linked with the lignin residues in the material. The existence of hemicellulose has been confirmed by the peaks positioned at 1304cm^{-1} (CH_2 stretching) and 1239cm^{-1} (C=O stretching). Finally, the peak noted around 598cm^{-1} is attributed by the C-OH stretching of cellulose in the fiber. Multiple concomitant investigations also observed similar FT-IR signatures that described in this study [63]. Although, this chemical investigation was sufficient to validate all other chemical characterization outcomes. Different functional groups and associated chemical component of HCSF was tabulated in Table 4.

Table 4 Different functional groups and associated chemical component of HCSF

Peak positions	Functional group	Linked chemical component
3344	OH stretching	Cellulose
2916	CH stretching	Cellulose
2832	C–H stretching of alkanes	α-cellulose
2317	C≡C stretching	Wax
1611	C=O stretching	Lignin
1406	CH_2 stretching	Cellulose
1304	CH_2 bending	Hemicellulose
1239	C=O stretching	Hemicellulose
1021	C-OH stretching	Lignin
598	C-OH bending	Cellulose

3.7 SEM/ SEM-EDX observations

The surface roughness or coarseness of HCSF was detected by the high-resolution SEM images captured at four different magnifications as 250×, 500×, 1000×, and 2000× (Fig. 7 (a–d)). It is clear from the picture that the cementing elements such as hemicellulose and lignin are used to bind many of the fiber bundles together. The corresponding hemicellulose, lignin, wax, and other impurities are visualized as small patches on the surface (Fig. 7 (a–c)). Rarely smoothened area was found that might be owed by the existence of small amount of wax

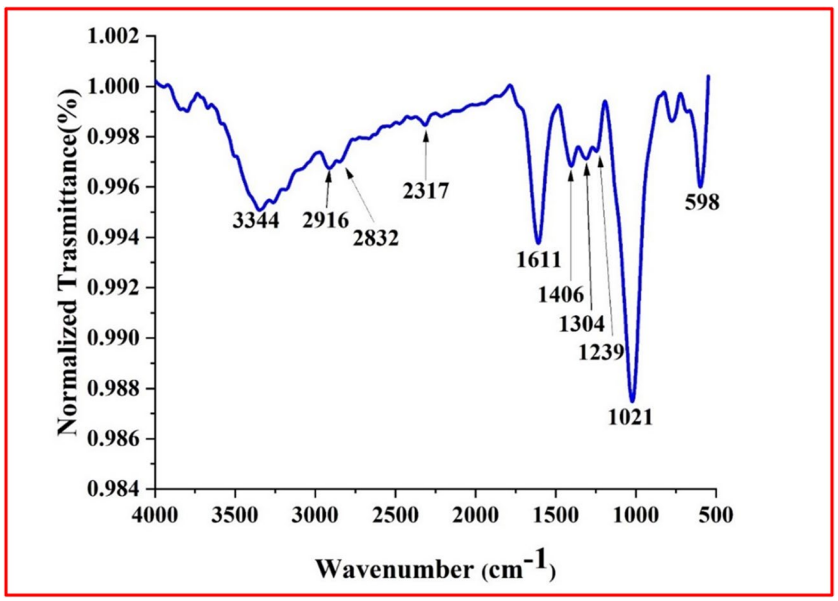

Fig. 6 FT-IR profile of HCSF

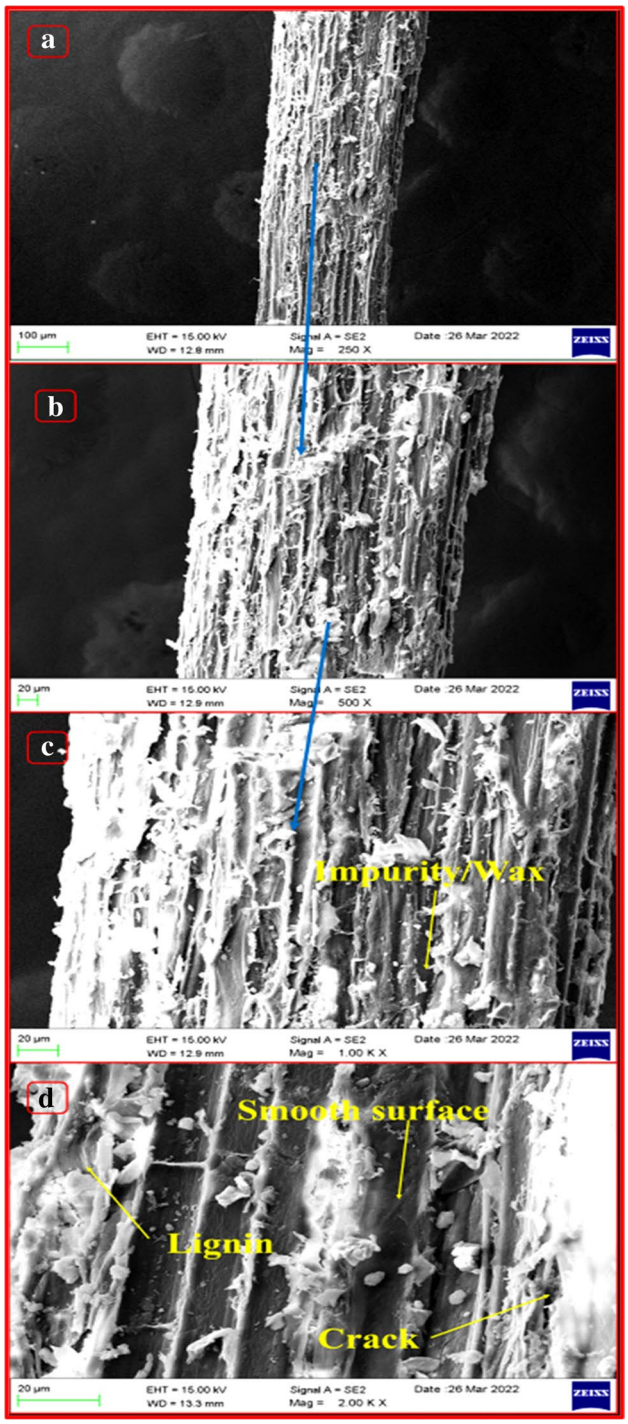

Fig. 7 (**a**, **b**, **c**, **d**) SEM images of HCSF at 250× (**a**), 500× (**b**), 1000× (**c**), and 2000× (**d**) magnification

and other impurities. Only fewer micro voids, holes, and fissures were observed, but uneven, mostly rough nature of the surface was noted as a most desired feature for inter-bonding with matrices. Figure 7(d) confirmed that the fiber posses good surface roughness since that can be a preferred option for composite preparation in future.

The energy-dispersive spectrogram of HCSF is seen in Fig. 8 (a, b); that revealed that there are three major elements are widely distributed on the fiber surface, which are carbon (C) and oxygen (O), and potassium (K). It is renowned that carbon and oxygen constitute the backbone of biomacromolecule like cellulose in all plants [64]. The prominence of potassium might be due to the existence of non-cellulosic materials on fiber surface. Moreover, few other elements were found to be in but minute quantities or negligible levels. This is due to contaminations or amorphous fractions present on its surface [24]. Presence of different elements on the surface of HCSF is provided in Table 5.

3.8 Roughness parameters of HCSF

Figure 9 (a–d) shows 2D/3D pictures, line profile, and specific roughness features of HCSF. Of which, 2D/3D images and line contour clearly present the roughness profile of HCSF that is favorable for appropriate fiber–matrix adhesion. Figure 9(d) explore the specific roughness properties of HCSF. The average roughness (R_a) of the fiber is identified as 7.2 nm, which was higher than the average roughness of *Symphirema involucratum* (6.647nm) [65]. The negative R_{sk} value (−0.528) indicates that the fiber surface has very little holes or fissures, that would provide a beneficial effect on creating interfacial bonds. Conversely, the required R_{ku} value (2.553) below 3 indicates that the fiber has good surface roughness [66, 67]. The remaining roughness parameters as R_z (33.937nm), R_t (42.624nm), and R_q (8.683nm) once again proved the roughness nature of fiber surface. These morphological topographies demonstrate that the surface roughness of HCSF is good as to consider it for composite formulations in future.

4 Conclusion

This study intended to identify a new plant fiber from *Hibiscus canescens* stem and to characterize it using standard protocols to establish its potential for use in polymeric composites. For that, plant stems were collected and soaked in water for an allotted amount of time to extract the fibers of interest. Physical, chemical, morphological, thermal, and mechanical methods were then used to further characterize the samples. The chemical characterization studies were pertinent to establish the chemical nature of the material; which proved that the material partakes high cellulose content (68.46 wt.%), good crystallinity index (48.78%), desired crystallite size (1.59nm), and more crystalline fractions than amorphous fractions. It is also reflected in the

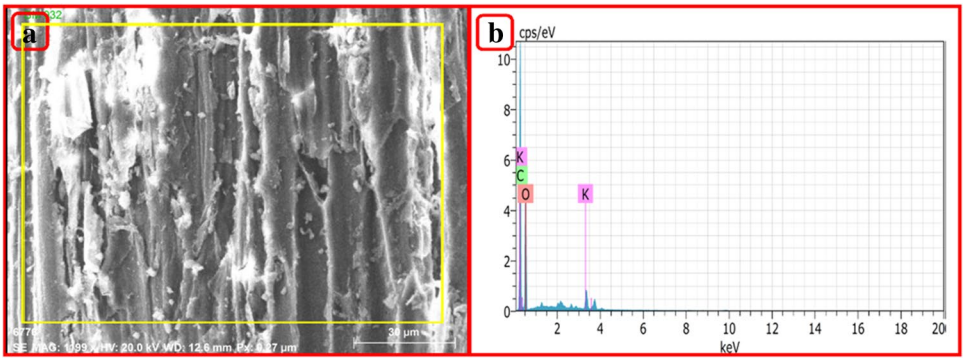

Fig. 8 (**a**, **b**) SEM-EDX image of HCSF (**a**) and relevant spectrogram (**b**)

Table 5 Presence of different elements on the surface of HCSF

Elements	Weight (%)	Atomic (%)
Carbon (C)	49.42	56.29
Oxygen (O)	49.29	42.62
Potassium (K)	1.28	0.45

thermal and tensile profiles that the fiber's high cellulosic crystalline fractions leads to good thermal stability (375°C) and tensile properties (394.9±14.42 MPa; 30.29±4.365 GPa). Along with this, low moisture content (10.44 wt.%) noted revealed that the fibers are strong enough to resist water or microbial attack. The density of the HCSF (1425 kg/m^3) is sufficient to ponder it for lightweight and structural applications. The topographical examination revealed rough surface of HCSF with an average roughness of 7.200nm that guaranteeing strong adhesion qualities while composite fabrication. Hence, the current study recommends the extensive utilization of *H. canescens* stem fiber for composite based applications in future.

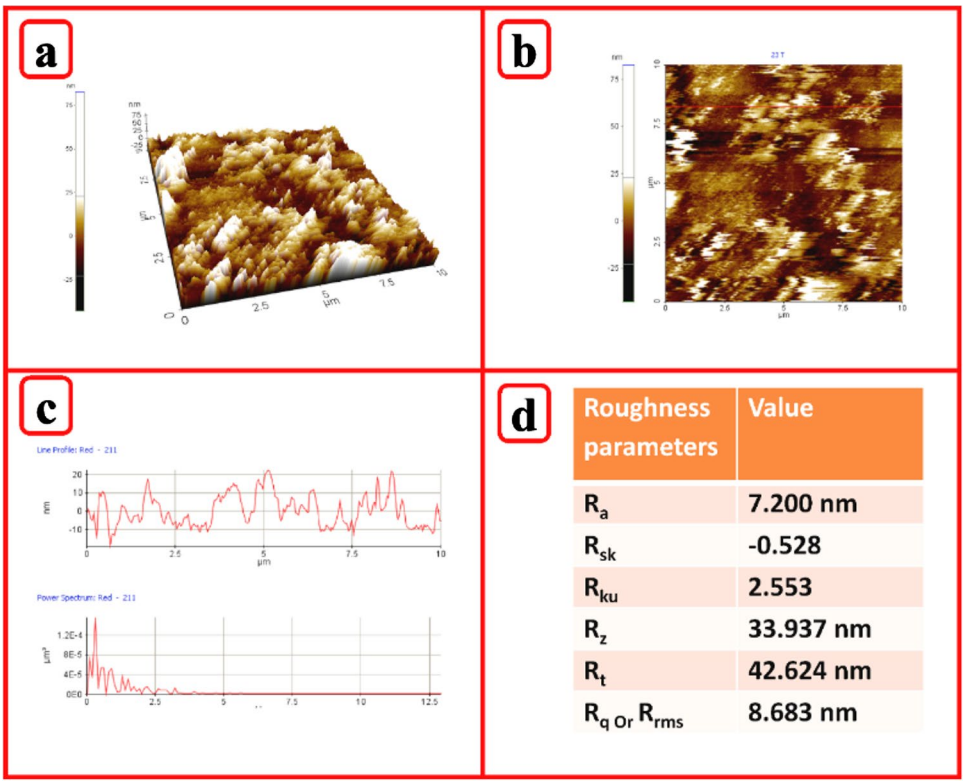

Fig. 9 (**a**, **b**, **c**, **d**) 2D/3D AFM images (**a**, **b**), line profile (**c**), and roughness parameters (**d**) of HCSF

Author contributions Raghuram Pradhan: investigation, formal analysis, writing original draft; Basanta Kumar Palai: methodology, visualization, manuscript editing and review and supervision; Dhirendra Nath Thatoi: formal analysis and resources; A. Elayaperumal; conceptualization; Japhia Sudarsan Nalla: validation.

Declarations

Ethical approval Not applicable.

Competing interests The authors declare no competing interests.

References

1. Arul Marcel Moshi A, Ravindran D, Sundara Bharathi SR et al (2020) Characterization of natural cellulosic fiber extracted from *Grewia damine* flowering plant's stem. Int J Biol Macromol 164:1246–1255. https://doi.org/10.1016/j.ijbiomac.2020.07.225
2. Ortega F, Versino F, López OV, García MA (2021) Biobased composites from agro-industrial wastes and by-products. Springer International Publishing
3. Indran S, Edwin Raj R, Sreenivasan VSS (2014) Characterization of new natural cellulosic fiber from *Cissus quadrangularis* root. Carbohydr Polym 110:423–429. https://doi.org/10.1016/j.carbpol.2014.04.051
4. Divya D, Suyambulingam I, Sanjay MR, Siengchin S (2022) Suitability examination of novel cellulosic plant fiber from *Furcraea selloa* K. Koch peduncle for a potential polymeric composite reinforcement. Polym Compos 43:4223–4243. https://doi.org/10.1002/PC.26683
5. Rangappa SM, Siengchin S, Parameswaranpillai J et al (2022) Lignocellulosic fiber reinforced composites: progress, performance, properties, applications, and future perspectives. Polym Compos 43:645–691. https://doi.org/10.1002/pc.26413
6. Hyness NRJ, Vignesh NJ, Senthamaraikannan P, Saravanakumar SS, Sanjay MR (2018) Characterization of new natural cellulosic fiber from *Heteropogon contortus*. Plant. Journal of Natural Fibers 15(1):146–153. https://doi.org/10.1080/15440478.2017.1321516
7. Binoj JSS, Raj REE, Indran S (2018) Characterization of industrial discarded fruit wastes (*Tamarindus indica* L.) as potential alternate for man-made vitreous fiber in polymer composites. Process Saf Environ Prot 116:527–534. https://doi.org/10.1016/j.psep.2018.02.019
8. Babu BG, Princewinston D, Saravanakumar SS et al (2020) Investigation on the physicochemical and mechanical properties of novel alkali-treated *Phaseolus vulgaris* fibers. J Nat Fibers 0478:1–13. https://doi.org/10.1080/15440478.2020.1761930
9. Divya D, Jenish I, Raja S (2022) Comprehensive characterization of *Furcraea selloa* K. Koch peduncle fiber-reinforced polyester composites — effect of fiber length and weight ratio. Adv Mater Sci Eng 2022:1–10
10. Sundaram RS, Rajamoni R, Suyambulingam I, Isaac R (2021) Comprehensive characterization of industrially discarded cymbopogon flexuosus stem fiber reinforced unsaturated polyester composites: effect of fiber length and weight fraction. J Nat Fibers 00:1–16. https://doi.org/10.1080/15440478.2021.1944435
11. Muthu Chozha Rajan B, Indran S, Divya D et al (2020) Mechanical and thermal properties of *Chloris barbata* flower fiber/epoxy composites: effect of alkali treatment and fiber weight fraction. J Nat Fibers 00:1–14. https://doi.org/10.1080/15440478.2020.1848703
12. Sari NH, Suteja IRA et al (2021) Characterization of the density and mechanical properties of corn husk fiber reinforced polyester composites after exposure to ultraviolet light. Funct Compos Struct 3:034001. https://doi.org/10.1088/2631-6331/ac0ed3
13. Raja S, Rajesh R, Indran S, Divya D (2021) Characterization of industrial discarded novel *Cymbopogon flexuosus* stem fiber: a potential replacement for synthetic fiber. J Ind Text 51:1207S–1234S. https://doi.org/10.1177/15280837211007507
14. Manimekalai G, Kavitha S, Divya D et al (2021) Characterization of enzyme treated cellulosic stem fiber from *Cissus quadrangularis* plant: an exploratory investigation. Curr Res Green Sustain Chem 4:100162. https://doi.org/10.1016/j.crgsc.2021.100162
15. Han X, Ding L, Tian Z, Song Y, Xiong R, Zhang C, Han J, Jiang S (2023) Potential new material for optical fiber: preparation and characterization of transparent fiber based on natural cellulosic fiber and epoxy. Int J Biol Macromol 224:1236–1243, ISSN 0141-8130. https://doi.org/10.1016/j.ijbiomac.2022.10.209
16. Maheshwaran MV, Hyness NRJ, Senthamaraikannan P, Saravanakumar SS, Sanjay MR (2018) Characterization of natural cellulosic fiber from *Epipremnum aureum* stem. J Nat Fibers 15(6):789–798. https://doi.org/10.1080/15440478.2017.1364205
17. Kumar R, Hynes NRJ, Senthamaraikannan P, Saravanakumar S, Sanjay MR (2018) Physicochemical and thermal properties of *Ceiba pentandra* bark fiber. J Nat Fibers 15(6):822–829. https://doi.org/10.1080/15440478.2017.1369208
18. Joe MS, Sudherson DPS, Suyambulingam I et al (2023) Extraction and characterization of novel biomass–based cellulosic plant fiber from *Ficus benjamina* L. stem for a potential polymeric composite reinforcement. Biomass Conv Bioref. https://doi.org/10.1007/s13399-023-03759-z
19. Karakoti A, Sunanda Biswas J, Aseer R, Sindhu N, Sanjay MR (2020) Characterization of microfiber isolated from *Hibiscus sabdariffa* var. *altissima* fiber by steam explosion. J Nat Fibers 17(2):189–198. https://doi.org/10.1080/15440478.2018.1477085
20. Senthamaraikannan P, Sanjay MR, Subrahmanya Bhat K, Padmaraj NH, Jawaid M (2019) Characterization of natural cellulosic fiber from bark of *Albizia amara*. J Nat Fibers 16(8):1124–1131. https://doi.org/10.1080/15440478.2018.1453432
21. Balavairavan B, Saravanakumar SS, Senthamaraikannan P et al (2023) Evaluation of physiochemical, mechanical, thermal, UV barrier, and biodegradation properties of PVA/corn (*Zea mays*) cob powder biofilms. Biomass Conv Bioref. https://doi.org/10.1007/s13399-023-04404-5
22. Bourmaud A, Shah DU, Beaugrand J, Dhakal HN (2020) Property changes in plant fibres during the processing of bio-based composites. Ind Crop Prod 154. https://doi.org/10.1016/j.indcrop.2020.112705
23. T.G. Yashas Gowda, M.R. Sanjay, K. Subrahmanya Bhat, P. Madhu, P. Senthamaraikannan & B. Yogesha. (2018) Polymer matrix-natural fiber composites: an overview, Cogent Eng, 5: 1, Duc Pham (Reviewing Editor) DOI: https://doi.org/10.1080/23311916.2018.1446667
24. Madhu P, Sanjay MR, Senthamaraikannan P, Pradeep S, Saravanakumar SS, Yogesha B (2019) A review on synthesis and characterization of commercially available natural fibers: Part II. J Nat Fibers 16(1):25–36. https://doi.org/10.1080/15440478.2017.1379045
25. Jotiram GA, Palai BK, Bhattacharya S et al (2022) Investigating mechanical strength of a natural fibre polymer composite using SiO2 nano-filler. Mater Today Proc 56:1522–1526. https://doi.org/10.1016/j.matpr.2022.01.176
26. Keke D, Cheng Y, Enhui S, Hongying H, Ping Q, Yueding X, Ling C, Qian S, Mingjie G (2022) Properties of bio-pretreated straw fiber and its composite materials. J Zhejiang A&F Univ 39(4):869–875. https://doi.org/10.11833/j.issn.2095-0756.20210647
27. Ding L, Han X, Cao L, Chen Y, Ling Z, Han J, He S, Jiang S (2022) Characterization of natural fiber from manau rattan

(*Calamus manan*) as a potential reinforcement for polymer-based composites. J Bioresour Bioprod 7(3):190–200, ISSN 2369-9698,. https://doi.org/10.1016/j.jobab.2021.11.002
28. Conrad CM (1944) Determination of wax in cotton fiber: a new alcohol extraction method. Ind Eng Chem 16:745–748
29. Khalil HPSA, Tehrani MA, Davoudpour Y et al (2013) Natural fiber reinforced poly(vinyl chloride) composites: a review. J Reinf Plast Compos 32:330–356. https://doi.org/10.1177/0731684412458553
30. Divakaran D, Sriariyanun M, Basha SA et al (2023) Physico-chemical, thermal, and morphological characterization of biomass-based novel microcrystalline cellulose from *Nelumbo nucifera* leaf: Biomass to biomaterial approach. Biomass Conv Bioref. https://doi.org/10.1007/s13399-023-04349-9
31. Han X, Ding L, Tian Z, Weijie W, Jiang S (2021) Extraction and characterization of novel ultrastrong and tough natural cellulosic fiber bundles from manau rattan (*Calamus manan*). Ind Crop Prod 173:114103, ISSN 0926-6690. https://doi.org/10.1016/j.indcrop.2021.114103
32. Indran S, Raj REE, Daniel BSSSS, Saravanakumar SSS (2016) Cellulose powder treatment on *Cissus quadrangularis* stem fiber-reinforcement in unsaturated polyester matrix composites. J Reinf Plast Compos 35:212–227. https://doi.org/10.1177/0731684415611756
33. Iyyadurai J, Arockiasamy FS, Manickam TS et al (2023) Revolutionizing polymer composites: boosting mechanical strength, thermal stability, water resistance, and sound absorption of cissus quadrangularis stem fibers with nano silica. Silicon. https://doi.org/10.1007/s12633-023-02510-7
34. Sutivisedsak N, Cheng HN, Burks CS et al (2012) Use of nutshells as fillers in polymer composites. J Polym Environ 20:305–314. https://doi.org/10.1007/s10924-012-0420-y
35. Imai T, Putaux JL, Sugiyama J (2003) Geometric phase analysis of lattice images from algal cellulose microfibrils. Polymer 44:1871–1879. https://doi.org/10.1016/s0032-3861(02)00861-3
36. Narayanasamy P, Balasundar P, Senthil S et al (2020) Characterization of a novel natural cellulosic fiber from *Calotropis gigantea* fruit bunch for ecofriendly polymer composites. Int J Biol Macromol 150:793–801. https://doi.org/10.1016/j.ijbiomac.2020.02.134
37. Mohan SJ, Devasahayam PSS, Suyambulingam I, Siengchin S (2022) Suitability characterization of novel cellulosic plant fiber from *Ficus benjamina* L. aerial root for a potential polymeric composite reinforcement. Polym Compos:1–15. https://doi.org/10.1002/pc.27080
38. Sunesh NP, Indran S, Divya D, Suchart S (2022) Isolation and characterization of novel agrowaste-based cellulosic micro fillers from *Borassus flabellifer* flower for polymer composite reinforcement. Polym Compos 43:6476–6488. https://doi.org/10.1002/pc.26960
39. Ramasamy S, Karuppuchamy A, Jayaraj JJ et al (2022) Comprehensive characterization of novel Robusta (AAA) banana bracts fibers reinforced polylactic acid based biocomposites for lightweight applications. Polym Compos:1–12. https://doi.org/10.1002/pc.27025
40. Edayadulla N, Divakaran D, Chandraraj SS et al (2023) Suitability study of novel bio-plasticizer from *Agave sisalana* leaf for biofilm applications: a biomass to biomaterial approach. Biomass Conv Bioref. https://doi.org/10.1007/s13399-023-04172-2
41. Somasundaram R, Rajamoni R, Suyambulingam I et al (2022) Utilization of discarded *Cymbopogon flexuosus* root waste as a novel lignocellulosic fiber for lightweight polymer composite application. Polym Compos 43:2838–2853. https://doi.org/10.1002/pc.26580
42. Divakaran D, Sriariyanun M, Jagadeesan R et al (2023) Isolation and characterization of an agro-industrial waste-based novel cellulosic micro fillers from mustard (*Brassica juncea*) seed oil cake: a waste to wealth approach. Biomass Conv Bioref. https://doi.org/10.1007/s13399-023-04346-y
43. Narayana Perumal S, Suyambulingam I, Divakaran D et al (2023) Extraction and physico-mechanical and thermal characterization of a novel green bio-plasticizer from *Pedalium murex* plant biomass for biofilm application. J Polym Environ. https://doi.org/10.1007/s10924-023-02898-8
44. Sarikanat M, Seki Y, Sever K, Durmuşkahya C (2014) Determination of properties of *Althaea officinalis* L. (marshmallow) fibres as a potential plant fibre in polymeric composite materials. Compos B Eng 57:180–186. https://doi.org/10.1016/j.compositesb.2013.09.041
45. Senthamaraikannan P, Saravanakumar SS, Arthanarieswaran VP (2016) Physico-chemical properties of new cellulosic fibers from the bark of *Acacia planifrons*. Int J Polym Anal Charact 21:207–213. https://doi.org/10.1080/1023666X.2016.1133138
46. Gopinath R, Ganesan K, Saravanakumar SS, Poopathi R (2016) Characterization of new cellulosic fiber from the stem of *Sida rhombifolia*. Int J Polym Anal Charact 21:123–129. https://doi.org/10.1080/1023666X.2016.1117712
47. Moshi AAM, Ravindran D, Bharathi SRSRS et al (2020) Characterization of a new cellulosic natural fiber extracted from the root of *Ficus religiosa* tree. Int J Biol Macromol 142:212–221. https://doi.org/10.1016/j.ijbiomac.2019.09.094
48. Priyadharshini GS, Velmurugan T, Suyambulingam I et al (2023) Characterization of cellulosic plant fiber extracted from *Waltheria indica* Linn. stem. Biomass Conv Bioref. https://doi.org/10.1007/s13399-023-04270-1
49. Maache M, Bezazi A, Amroune S et al (2017) Characterization of a novel natural cellulosic fiber from *Juncus effusus* L. Carbohydr Polym 171:163–172. https://doi.org/10.1016/j.carbpol.2017.04.096
50. Kavimani V, Divakaran D, Sriariyanun M et al (2023) Facile exfoliation and physicochemical characterization of biomass-based cellulose derived from *Pandanus tectorius* leaves for sustainable environment. Biomass Conv Bioref. https://doi.org/10.1007/s13399-023-04187-9
51. Seki Y, Sarikanat M, Sever K, Durmus C (2013) Extraction and properties of *Ferula communis* (chakshir) fibers as novel reinforcement for composites materials. Composites: Part B 44:517–523. https://doi.org/10.1016/j.compositesb.2012.03.013
52. Kathiresan M, Pandiarajan P, Senthamaraikannan P, Saravanakumar SS (2016) Physicochemical properties of new cellulosic *Artisdita hystrix* leaf fiber. Int J Polym Anal Charact 21:663–668. https://doi.org/10.1080/1023666X.2016.1194636
53. Teixeira EDM, Corre AC, Manzoli A et al (2010) Cellulose nanofibers from white and naturally colored cotton fibers. Cellulose 17:595–606. https://doi.org/10.1007/s10570-010-9403-0
54. Jebadurai SG, Raj RE, Sreenivasan VS, Binoj JS (2019) Comprehensive characterization of natural cellulosic fiber from *Coccinia grandis* stem. Elsevier Ltd.
55. Shanmugasundaram N, Rajendran I, Ramkumar T (2018) Characterization of untreated and alkali treated new cellulosic fiber from an *Areca* palm leaf stalk as potential reinforcement in polymer composites. Carbohydr Polym 195:566–575. https://doi.org/10.1016/j.carbpol.2018.04.127
56. Pratheesh K, Narayanasamy P, Prithivirajan R et al (2023) Cenosphere filled epoxy composites: structural, mechanical, and dynamic mechanical studies. Biomass Conv Bioref. https://doi.org/10.1007/s13399-023-04154-4
57. Kathirselvam M, Kumaravel A, Arthanarieswaran VP, Saravanakumar SS (2019) Characterization of cellulose fibers in *Thespesia populnea* barks: influence of alkali treatment. Carbohydr Polym 217:178–189. https://doi.org/10.1016/j.carbpol.2019.04.063
58. Kaushik A, Singh M, Verma G (2010) Green nanocomposites based on thermoplastic starch and steam exploded cellulose nanofibrils from wheat straw. Carbohydr Polym 82:337–345. https://doi.org/10.1016/j.carbpol.2010.04.063
59. Asim M, Jawaid M, Abdan K, Ishak MR (2016) Effect of alkali and silane treatments on mechanical and fibre-matrix bond

strength of kenaf and pineapple leaf fibres. J Bionic Eng 13:426–435. https://doi.org/10.1016/S1672-6529(16)60315-3
60. Sathishkumar TP, Navaneethakrishnan P, Shankar S et al (2013) Characterization of natural fiber and composites - a review. J Reinf Plast Compos 32:1457–1476. https://doi.org/10.1177/0731684413495322
61. Gandhi VCS, Jenish I, Indran S, Rajan DY (2022) Mechanical and thermal analysis of *Cissus quadrangularis* stem fiber/epoxy composite with micro-red mud filler composite for structural application. Trans Indian Inst Metals 75:737–747. https://doi.org/10.1007/s12666-021-02478-1
62. Durai PN, Viswalingam K, Divya D, Senthilkumar B (2022) Mechanical, thermal, and surface morphological properties of *Musa acuminate* peduncle fiber-reinforced polymeric composite: effect of alkalization and fiber loading. Polym Compos 43:5107–5118. https://doi.org/10.1002/pc.26800
63. Manimaran P, Jeyasekaran AS, Purohit R et al (2020) An experimental and numerical investigation on the mechanical properties of addition of wood flour fillers in red banana peduncle fiber reinforced polyester composites. J Nat Fibers 17:1140–1158. https://doi.org/10.1080/15440478.2018.1558148
64. Rantheesh J, Indran S, Raja S et al (2023) Isolation and characterization of novel micro cellulose from *Azadirachta indica* A. Juss agro-industrial residual waste oil cake for futuristic applications. Biomass Conv Bioref 13:4393–4411. https://doi.org/10.1007/s13399-022-03467-0
65. Raju JSN, Depoures MV, Kumaran P (2021) Comprehensive characterization of raw and alkali (NaOH) treated natural fibers from *Symphirema involucratum* stem. Int J Biol Macromol 186:886–896. https://doi.org/10.1016/j.ijbiomac.2021.07.061
66. Alshammari BA, Alotaibi MD, Alothman OY et al (2019) A new study on characterization and properties of natural fibers obtained from olive tree (*Olea europaea* L.) residues. J Polym Environ 27:2334–2340. https://doi.org/10.1007/s10924-019-01526-8
67. Indran S, Divya D, Raja S, Sanjay MR, Siengchin S (2023) Physico-chemical, mechanical and morphological characterization of *Furcraea selloa* K. Koch plant leaf fibers-an exploratory investigation. J Nat Fibers 20:1. https://doi.org/10.1080/15440478.2022.2146829